Adaptive Antitumor Immune Response Stimulated by Bio-nanoparticle Based Vaccine and Checkpoint Blockade

Xuewei Bai
Liver Research Center, RI Hospital and the Warren Alpert Medical School of Brown University
Yanmei Zhou
Liver Research Center, RI Hospital and the Warren Alpert Medical School of Brown University
Yuki Yokota
Liver Research Center, RI Hospital and the Warren Alpert Medical School of Brown University
Yoshihiro Matsumoto
Liver Research Center, RI Hospital and the Warren Alpert Medical School of Brown University
Bo Zhai
Liver Research Center, RI Hospital and the Warren Alpert Medical School of Brown University
Nader Maarouf
Liver Research Center, RI Hospital and the Warren Alpert Medical School of Brown University
Hikaru Hayashi
Liver Research Center, RI Hospital and the Warren Alpert Medical School of Brown University
Rolf Carlson
Rhode Island Hospital
Songhua Zhang
Liver Research Center, RI Hospital and the Warren Alpert Medical School of Brown University
Aryanna Sousa
Liver Research Center, RI Hospital and the Warren Alpert Medical School of Brown University
Bei Sun
The First Affiliated Hospital of Harbin Medical University
Hossein Ghanbari
Athanor Biosciences Inc.
Xiaoqun Dong
Liver Research Center, RI Hospital and the Warren Alpert Medical School of Brown University
Jack R Wands (jack_wands_md@brown.edu)
Liver Research Center, RI Hospital and the Warren Alpert Medical School of Brown University

Research Article

Keywords: Aspartate β-hydroxylase (ASPH), immune checkpoint inhibitor, lambda phage vaccine, cancer metastasis

Posted Date: October 18th, 2021

DOI: https://doi.org/10.21203/rs.3.rs-966722/v1

Version of Record: A version of this preprint was published at Journal of Experimental & Clinical Cancer Research on April 8th, 2022. See the published version at https://doi.org/10.1186/s13046-022-02307-3.

Abstract

Background: Interactions between tumor and microenvironment determines the response to immunotherapy. Triple negative breast cancer (TNBC) and hepatocellular carcinoma (HCC) have exhibited suboptimal responses to immune checkpoint inhibitors. Aspartate beta-hydroxylase (ASPH), an oncofetal protein and tumor associated antigen (TAA), is a potential target for immunotherapy.

Methods: Orthotopic TNBC and subcutaneous HCC murine models were established. Immunohistochemistry, flow cytometry, ELISA and *in vitro* cytotoxicity assays were performed.

Results: The ASPH-MYC signaling cascade upregulates PD-L1 expression on breast and liver tumor cells. A bio-nanoparticle based vaccine targeting ASPH was administrated to BALB/c mice harboring syngeneic HCC or TNBC tumors, either alone or in combination with PD-1 blockade. In the control group, autocrine CXCL13-CXCR5 axis promoted cancer development and progression. Inhibition between PD-L1$^+$ cancer cells and PD-1$^+$ T cells resulted in T cell exhaustion and apoptosis. In contrast, combination therapy significantly suppressed primary hepatic or mammary tumor growth with distant pulmonary metastases in TNBC. An adaptive immune response was attributed to expansion of activated CD4$^+$ Th1/CD8$^+$ CTLs with enhanced effector function and high titers of ASPH-specific antibody. When the PD-1/PD-L1 signal was inhibited, CXCL13 produced by ASPH$^+$ cancer cells recruited CXCR5$^+$/CD8$^+$ T lymphocytes to tertiary lymphoid structures (TLSs), which secreted CXCL13 to recruit more CXCR5$^+$ immune cells and to lyse CXCR5$^+$ cancer cells. Upon combination treatment, the presence of TLSs predicts sensitivity to immune checkpoint inhibitor blockade.

Conclusions: Synergistic antitumor efficacy attributable to a λ phage vaccine specifically targeting ASPH combined with an immune checkpoint inhibitor represents a new approach for TNBC and HCC.

Background

Malignancy is the second (16.7%) leading cause of death globally and is responsible for an estimated 9.6 million deaths in 2018. By 2040, the global burden is expected to reach 27.5 million new cases with an associated 16.3 million deaths. Despite advancements in surgery, chemotherapy, radiotherapy and targeted therapy, 782,000 people died of liver cancer (hepatocellular carcinoma [HCC) whereas 627,000 people died of breast cancer in 2018 world-wide(1). Therefore, it is essential to develop immunologic approaches in an attempt to treat such aggressive and refractory oncologic diseases. Triple negative breast cancer (TNBC) has a highly metastatic phenotype and primary HCC are relatively resistant to checkpoint inhibitor blockade alone. The recent emergence of checkpoint inhibitors in combination with immune stimulation has provided direct evidence that the immune system may be a therapeutic modulator of tumor development and progression.

Immune checkpoint inhibitor blockade is an attractive strategy of cancer therapeutics involving modulation of the cellular interactions in the tumor-microenvironment (TME). The checkpoint inhibitors,

such as CTLA4, PD-1 and PD-L1 antibodies, have become important new therapeutic agents. The PD-1/PD-L1 pathways are mediators of tumor-induced immunosuppression. In this context, PD-1/PD-L1 signals controls inflammation at locations expressing specific antigens to prevent and protect normal tissue from damage. When a T cell recognizes a neo-antigen presented by the MHC complex on a target cell, inflammatory cytokines are produced, initiating a pro-inflammatory response. These cytokines upregulate PD-L1 expression on the tumor target cell and binds to the PD-1 expressed on the T cell, leading to anergy and immune tolerance; a phenomenon where the immune system loses control to mount an inflammatory response, even in the presence of neo-antigen exposure. This protective mechanism is circumvented by tumor cells via upregulation of PD-L1 expression to blunt the host immune response. The PD-1/PD-L1 inhibitors are pharmacologically designed to prevent PD-1/PD-L1 interactions, thus releasing an adaptive immune response to promote tumor cell lysis(2).

In view of the known efficacy of anti-PD1/anti-PD-L1 therapy, there appears to be only a few tissue types of cancers that are susceptible to this approach. Thus far, immune checkpoint inhibitors have exhibited little or no activity in subsets of tumors with lower mutational burdens, such as Ewing sarcoma and prostate cancer. Furthermore, in an unselected subpopulation of patients with colorectal tumors, PD-1 inhibitors have little or no efficacy(3). Pembrolizumab (Keytruda®) was granted FDA approval for treatment of certain patients with advanced HCC since there are approximately 42,030 new cases and 31,780 deaths from this disease in the United States alone in 2019. Moreover, there are limited options in advanced HCC since phase 3 Keytruda® trials failed in HCC patients who had previously received Sorafenib (Nexavar) a multiple kinase inhibitor. The discovery and use of certain target antigens may boost the immune response if combined in a vaccine construct with checkpoint inhibitor blockade to achieve anti-tumor effects not present in resistant tumors.

The ASPH is a transmembrane β-hydroxylase(4), highly conserved during mammalian evolution. It is expressed in the embryo during early development but silenced at birth and during adulthood. It is only reactivated when oncogenesis has been initiated(4, 5) a process where it translocates to the cell surface membrane, where N and C-terminal regions are exposed to the extracellular environment. Subsequently, ASPH interact with the immune system and serves as a tumor associated antigen (TAA) stably presented on a broad spectrum of tumor tissue types and represents an ideal target for immunotherapy. Importantly, antigenic epitopes that reside on the extracellular regions of ASPH efficiently stimulate antigen specific T-cell responses to a variety of expressing tumor tissue types(6). Previous studies have established that ASPH is a target for immunotherapy using a dendritic cell (DC) vaccine approach in syngeneic animal models of HCC and cholangiocarcinoma(7, 8).

Activation of RAS/ERK, PI3K/AKT and WNT/β-catenin signals are known to upregulate transcription of the ASPH gene, which contributes to tumorigenesis by promoting tumor cell proliferation, migration, invasion(5, 9) and metastasis(10–12). Its oncogenic properties(12–15) are due to: 1) activation of the Notch(16, 17) and SRC(12) cascades; 2) inhibit apoptosis; 3) promote dysregulation of cell cycle control; 4) induce of cell senescence; and 5) promote a gain of a cancer stem cell phenotype. In combination, these processes are necessary and sufficient for the spontaneous development, growth and progression

of HCC in a double transgenic murine model(18). Therefore, targeting this oncogenic network may have therapeutic potential(19).

Immunotherapy is particularly attractive approach since ASPH: 1) is a transmembrane protein with high expression on cell surface in various malignancies; 2) expresses at extremely low or negligible levels in normal human tissues except in placenta, which is a highly invasive tissue; 3) has a defined pro-oncogenic role by promoting migration and invasion of tumor cells; 4) approximately 85% of hepatitis C virus (HCV) and hepatitis B virus (HBV) related HCC, as well as >85% of breast cancers, and especially in triple negative (TNBC) and HER2 amplified subtypes(16), which also exhibits upregulation of the ASPH gene(20). In addition, moderate to high level expression of ASPH portends a worse surgical outcome(20), and predicts a more aggressive clinical course (20, 21). ASPH overexpression is also associated with early disease reoccurrence, and subsequently reduces overall disease-free survival(16).

Immune contexture(22–25) of the TMI has been linked to host survival of certain tumor subtypes. The contexture evaluates various components infiltrating the tumor as an integrated system and defines the interconnected elements. Immune contexture is comprised and characterized by an immunoscore of tumor infiltrating lymphocytes (TILS) based on (1) type; (2) density; (3) anatomic site, (4) intratumoral location; (5) composition of different subpopulations (especially CD8+/CD62L+ effector T and CD45RO+ memory T); (6) functional orientation of the secretome derived from T helper type 1 (TH1) cells (e.g., IFN-γ) and CTLs (e.g., granzymes, perforin, granulysin); and (7) organizational pattern (scattered vs. clustered) and spatial distribution (relationship with the tumor and adjacent vasculature/lymphatic system) of immune cells within a tumor.

Tertiary lymphoid structures (TLSs) are ectopic aggregates indicating cellular neogenesis in non-lymphoid tissues at the site of inflammation and tumor growth(26–28). Tumor associated TLSs are typically located peritumorally with morphological, cellular and molecular similarity to secondary lymphoid organs, such as lymph nodes. The TLSs are composed of a T cell zone containing mature DC-Lamp+ dendritic cells (DCs), adjacent to a B cell zone which includes a typical germinal center (GC) comprising B cells embedded within a network of follicular DC (FDC). There are PNAd+ high endothelial venules (HEV) surround TLS, enabling lymphocyte entry to and from the blood. It is likely that the presence of TLSs may predict tumor responses to immunotherapy.

Bacteriophages are viruses that infect certain bacterial hosts. Bacteriophages are attractive candidates for vaccine delivery due to their high stability in harsh environments, as well as ease for large-scale production, and most importantly, serve as potent adjuvants to enhance the host immune responses to the immunizing antigen(29, 30). Bacteriophage display is a favorable approach to present peptides to the immune system. The lambda (λ) phage contains a linear double-stranded DNA (dsDNA) genome, which can be modified for antigen display, an advantage over filamentous phages(31). Because λ phage is assembled in the cytoplasm, it is particularly well-suited for the display of cytoplasmic proteins and has the capability for multi-antigen presentation which may allow for further antigen selection and

amplification(32). Here we employ an ASPH-based l phage vaccine construct when used in combination with checkpoint inhibitors produces a more robust synergistic anti-tumor immune response.

Materials And Methods

Cell lines

The murine breast tumor cell line 4T1 (ATCC, CRL-2539) and liver HCC cell line BNL 1ME A.7R.1 (BNL) (ATCC, TIB-75) were cultured at 37°C in a humidified atmosphere containing 5% CO_2 in Dulbecco's modified Eagle's medium (DMEM) supplemented with 2mM L-glutamine, 10% FBS and antibiotics (penicillin and streptomycin).

Recombinant human ASPH protein preparation

The full length human *ASPH* gene (GenBank accession No. S83325) was cloned into the EcoRI site of the pcDNA vector (Invitrogen, Carlsbad, CA). Recombinant ASPH protein (rASPH) was produced in a Baculovirus Expression system (Invitrogen) according to manufacturer's instructions(6–8, 33).

Construction of bacteriophage λ to display ASPH peptides(33)

The ASPH-based λ phage vaccine (BNP-TV) was developed and synthesized in collaboration with investigators of Panacea Therapeutics(33). Bacteriophage λ was designed to display ASPH protein fused at the carboxyl terminus of the capsid protein gpD(33). This system applied both to the N and C-terminal regions of human ASPH protein, designated as ASPH construct λ1 and λ3, respectively. The N- and C-segments were amplified from *ASPH* gene using specific oligo primers by PCR; their sequences were modified to produce restriction sites for Nhe I and Bssh II enzymes. After restriction enzyme digestion, the *ASPH* segments were inserted at the NheI-BsshII site of the 3' end of DNA segment encoding gpD controlled by the Lac Operon. These constructs were established in donor plasmid pVCDcDL1A harboring *loxPwt* and *loxP511* sequences. Subsequently, Cre-expressing *E. coli* was transformed with recombinant plasmids and infected with recipient λ phage DL1 (λ-DL1) carrying DNA segment flanked by *loxPwt* and *loxP511* sites. Recombination *in vivo* at the *loxP* sites and cointegration with *Ampr* spontaneously lysed the *E. coli, which* released assembled "virions" to culture media. This cointegration produced recombinant λ phage to display ASPH peptides fused at the C-terminus of gpD. Recombination with unmodified pVCDcDL3 yielded control phage particles displaying no peptide(33).

Reagents

In vivo mAb anti-mouse PD-1 (CD279) (clone RMP1-14) was purchased from Bioxcell (Catalog #BE0146, West Lebanon, NH). The antibody was administered intraperitoneally (i.p.) either alone or in combination with λ phage vaccine.

Murine subcutaneous model of HCC and orthotopic model of TNBC

This study had been approved by the Institutional Animal Care and Use Committee at Rhode Island Hospital (Providence, RI). The experimental design is shown in Figure 1A. Female immunocompetent BALB/c mice aged 6-8-weeks-old (Charles River Laboratories, Wilmington, MA) were randomly assigned to 4 groups (n=10/group): control (empty phage construct + IgG isotype antibody), PD-1 blockade (treated with PD-1 inhibitor), vaccine (immunized with ASPH-based λ phage), and PD-1 blockade + vaccine (combination). The mice in the vaccine and combination groups were immunized once a week by subcutaneous injection 1×10^{10} pfu λ1 phage particles (expressing N-terminal human ASPH peptides) suspended in 50μl of sterile saline into the base of tail. BNL cells (1×10^{6}) or 4T1 cells (5×10^{4}) in 50μl (volume of cell suspension: Matrigel at 1:1) were subcutaneously inoculated into the right flank or the 4th mammary fat pad, respectively. The mice in vaccine and combination groups received a therapeutic schedule of λ phage vaccine once per week starting in 2 weeks after BNL cells were implanted and when the tumor was established. Simultaneously, in PD-1 blockade and combination groups, anti-PD-1 monoclonal antibody (12.5μg-200μg/mouse) was i.p. administered twice per week. Tumor size was measured(8, 33) using calipers 2–3 times per week and tumor volume was calculated as $(\text{length}\times\text{width}^2)/2$. Six to eight weeks (for HCC model) or 4 weeks (for TNBC model) after tumor cell inoculation, mice bearing tumors with the shorter diameter exceeded 10 mm were euthanized according to specific requirements from Animal Welfare Committee of the Rhode Island Hospital (Providence, RI). Primary tumors, spleen, lungs and other tissue samples were harvested and stored at −80°C. The number and size of macro-metastatic lesions in the lungs (immersed in Bouin's fixative solution) were counted and size determined. Tumors were excised and fixed with 10% formalin for hematoxylin & eosin (H&E) and immunohistochemistry (IHC) staining.

Isolation and characterization of murine splenocytes(33)

Following euthanasia, spleens were resected from mice bearing tumors in the four different groups and dispersed into a cell suspension using the plunger end from 3 ml syringe, followed by a filtering process with 70μm cell strainer. Erythrocytes were lysed with RBC lysis solution buffer (BD Biosciences, San Jose, CA). After isolation, splenocytes (1×10^{6} cells/ml) were cultured in RPMI-1640 (containing 10% FBS, 1 × non-essential amino acids, 1 × amino acid solution, 100 μM sodium pyruvate, 1 × penicillin-streptomycin and 2-Mercaptoethanol [50 μM]) and re-stimulated with 0.4-0.5μg/ml of recombinant protein (rASPH) and 2×10^{8} pfu/ml λ phage particles *in vitro* for 4 days(8, 33). Simultaneously, 10 ng/ml of IL-2 (PeproTech, Rocky Hill, NJ) was added for 2 days. Following the 4-day re-stimulation of splenocytes with λ phage and rASPH, the supernatants derived from culture media were collected for ELISA to quantify cytokine secretion. This assay was previously optimized for T cell activation using DCs pulsed with ASPH containing microparticles(6, 8). To remove dead cells from re-stimulated splenocytes, density-gradient centrifugation was performed using Lympholyte®-M (Cedarlane, Burlington, NC). Purified re-stimulated splenocytes were used for *in vitro* cytotoxicity assays and flow cytometric analysis.

In vitro Cytotoxicity

Briefly, BNL or 4T1 cells were co-cultured with isolated splenocyte suspension for 5h. A Cytotoxicity Detection Kit^{PLUS} (LDH) (Sigma-Aldrich, #4744926001) was applied to measure lymphocytic cytotoxicity(8, 33).

Flow cytometry

After isolation and re-stimulation, the splenocytes were collected, washed and immunophenotyped by using the following anti-mouse monoclonal antibodies: CD3-eFluor 450, CD4-FITC (Thermo Fisher Scientific), and CD8a-APC-H7 (BD Biosciences). Appropriate isotype controls were used for comparison. After staining, the splenocytes were assessed by BD FACSAria^{TM} II Flow Cytometer (BD Biosciences, San Jose, CA, USA). Dead cells were excluded by using a LIVE/DEAD Fixable Dead Cell Stain (Invitrogen). Antigen specific $CD4^+$ or $CD8^+$ T cells were analyzed with FlowJo software (Tree Star Inc., Ashland, OR) (33).

Enzyme-Linked Immunosorbent Assay (ELISA)

Whole blood (400μL) was collected from the heart after euthanasia and centrifuged at 3000 rpm for 20 min. Serum samples were collected following centrifugation and stored at -80°C. Interferon gamma (IFN-γ) ELISA Kit (Thermo Fisher Scientific, #KMC4021) was used to measure secretion levels in cell culture supernatants after serial dilutions (1:4). A total of 100μl of standard, control or serum/supernatant was added to each well and incubated for 2h at room temperature. The solution was thoroughly mixed, and each well was washed 4 times with 1× PBS buffer. Then, 100μl mouse IFN-γ biotin conjugate solution was added into each well and incubated for 1h at room temperature. Subsequently, 100μl 1× streptavidin-HRP solution was added into each well and incubated for 30 min at room temperature. Afterwards, each well was washed and 100μl stabilized chromogen was added. The absorbance was read at 450nm after adding stop solution. The concentration of each sample was calculated according to the standard curve.

IHC & Immunofluorescence (IF)

Tumor cells were seeded on coverslips embedded with glycine, fixed with 4% formaldehyde and stained. Tumor tissues were fixed in 4% formaldehyde, embedded in paraffin, and sectioned into 4-μm-thick slides. The antigen was retrieved, and endogenous peroxidase activity was quenched through a 30-min treatment in methanol with 3% hydrogen peroxide. Non-specific antigen was blocked for 1h. The slides were incubated with primary antibodies overnight at 4°C. After rinsing, HRP (Vector Laboratories, #PK4001 and #PK-6102) or fluorescent second antibody (Thermo Fisher Scientific, #RMG101 and #A24538) was added onto the slides and incubated for 1h. For IF, the slides were mounted with DAPI (Vector Laboratories, #H-1800) and observed under the fluorescence microscope. For IHC, the slides were incubated with peroxidase-label for 30 min, developed with DAB Kit (SK-4100, Vector Laboratories) and counterstained with hematoxylin. For quantitation, 5 microscopic fields were randomly selected at 400× magnification. Images were analyzed by NIH ImageJ software (https://imagej.nih.gov/ij/).

Tertiary lymphoid structures (TLSs)

The existence of intra-tumoral TLSs was assessed morphologically on H&E stained FFPE slides(34). Stained cells were counted semi-quantitatively (score 0, 1, 2, 3, and 4 for none, very low, weak, intermediate, and high density of positive cells, respectively) in each intermediate-power field (IPF) in intra- and peri-tumoral areas of the entire section (original magnification ×100) and expressed as mean scores ± SEMs per IPF. The numbers of DC-LAMP$^+$ mature DCs and CD8$^+$ T cells were counted and expressed as mean cells ± SEMs per IPF. Immunostaining of CD4, CD8, CD45RO, was semi-quantified as a percentage of positive cells among CD3$^+$ T cells. Necrosis was scored as the percent of the positive necrotic areas among the entire tumor section. Both immunostaining and scoring were evaluated by 3 independent observers.

Evaluation of tumor microenvironment

After deparaffinization, antigen retrieval and endogenous peroxidase blocking, immunohistochemical staining was performed using the VECTASTAIN Elite ABC kit (Vector Laboratories, Burlingame, CA) according to the manufacture's protocol. Primary antibodies were against ASPH (laboratory developed mouse monoclonal antibody [Alsaab, #2], diluted at 1:10000), PD-1 (ab214421), PD-L1 (ab213480), CD21 (ab75985) and CD19 (ab203615) purchased from Abcam; CD3 (MA5-14524), CD8 (14-0808-82), CD45RO (MA5-11532), BCL-6 (PA5-14259), DC-LAMP/CD208 (PA5-96217), LRP1 (37-7600) and TLR4 (710185) from purchased from Thermo Fisher Scientific. The FFPE sections were incubated with primary antibodies at 4°C overnight, then color development was performed using DAB Peroxidase Substrate (Vector Laboratories) for 60–90 seconds. Counterstaining was performed by hematoxylin. The CD3+ and CD8+ T cells were counted per randomly selected 5–10 high-power fields (400×) and CD45RO+ cells were counted in 10 fields (1000×) using NIH ImageJ software (Bethesda, MD). The mean number of CD3+, CD8+ or CD45+ T cells infiltrating the tumor parenchyma from 5 different sections derived from 3–5 tumors were calculated.

Statistical analysis

Statistical analysis was performed using SPSS software (version 22.0). Quantitative data was presented as means ± SEM and analyzed by one-way analysis of variance (ANOVA) (comparison among multiple groups, with Tukey *post hoc* or Kruskal–Wallis test, or with Dunn *post hoc* test for nonparametric comparison) as well as Student's *t*, unpaired Mann–Whitney *U* or v Fisher's Exact tests when appropriate (comparison between two groups). Equality of variance was examined using F-test. For tertiary lymphoid structures (TLS) assessment, immunostaining was manually annotated. IHC scores from different groups were compared by χ^2 or Fisher's Exact tests. A *p*-value of <0.05 (two-sided) was considered as statistically significant.

Results

ASPH-MYC axis upregulates PD-L1 surface expression on HCC cells.

It has been previously demonstrated that enhanced ASPH expression activates the Notch signal transduction cascade and upregulates downstream target genes, such as c-MYC, that participate in oncogenic process(14). The c-MYC gene expression has been observed to regulate PD-L1 expression(35, 36). Consequently, mice harboring “wild type” untreated BNL HCC demonstrate upregulation of the PD-L1 by the ASPH-MYC signaling cascade (Fig. 1A; **Additional File 1: Fig. S1A**) as demonstrated by IHC. Splenocytes derived from the combined treatment group also demonstrated cytotoxicity to TNBC breast cancer cells that have high endogenous expression of ASPH.

Phage vaccination targeting ASPH in combination with PD-1 blockade strikingly reduces HCC tumor growth and progression in a syngeneic subcutaneous murine model.

Combination therapy resulted in a substantial reduction in HCC development and growth compared to control as well as the PD-1 inhibitor and vaccine treatment groups. Tumor growth was blunted by either vaccine or PD-1 blockade alone, to an intermediate extent between control and combination therapy (**Additional File 1: Fig. S1B;** Fig. 1B-D). A substantial decrease in tumor volume of the excised HCC was attributed to combination therapy. Very little, if any, growth of the HCC was observed in response to combination therapy. In these tumors, 90% of the resultant tissue contained broad areas of necrosis and inflammation and very little viable tumor (data not shown).

Antigen specific activation of $CD4^+$ Th and $CD8^+$ CTLs was stimulated by ASPH-based λ phage vaccine immunization in combination with PD-1 blockade in the BNL derived HCC model.

To achieve potent anti-tumor effects, both $CD4^+$ Th and $CD8^+$ CTLs are involved(7, 8). An *in vitro* cytotoxicity assay that measures $CD8^+$ CTL cytotoxic activity was performed as previously described(8, 33). The BNL cells were seeded into a 96-well plate and allowed to attach for 1h. Subsequently, suspension of splenocytes derived from mice in different groups was added at a ratio of splenocytes to target (BNL) cells varying from 2:1, 10:1 to 20:1, respectively, and incubated with BNL cells for 4h. Lactate dehydrogenase (LDH) release from the lysed BNL cells was measured as an indicator of cytotoxic activity. There was a marked increase in CTL activity of splenocytes derived from the combination group when compared to control. Either anti-PD-1 or vaccine administration alone generated an intermediate response. The ASPH-based phage vaccination was as effective as PD-1 blockade with respect to lysis of BNL cells (Fig. 1E).

The *in vitro* cytotoxicity of splenocytes derived from the HCC model was evaluated in the context of the metastatic 4T1 breast cancer induced tumors as target cells with high endogenous overexpression of ASPH. It was observed that splenocytes derived from the BNL HCC group also substantially enhanced $CD8^+$ CTL activity against 4T1 breast cancer cells as compared to splenocytes derived from control animals (**Additional File 1: Fig. S1C**). Thus, splenocytes sensitized to ASPH *in vivo* can be used to lyse cells derived from other tumors that endogenously express ASPH.

The percent of ASPH specific $CD4^+$ Th and $CD8^+$ CTL activated in splenocyte populations was further analyzed by flow cytometry (Fig. 1F). The number of ASPH specific $CD4^+$ Th1 and $CD8^+$ CTL was substantially increased as measured by the secretion of IFN-γ after restimulation of splenocytes with ASPH-based λ phage vaccine and rASPH protein. The highest level of response was observed with combination therapy, compared to either λ phage vaccine or PD-1 blockade alone.

Histologic features of HCC varied significantly when comparing control to the other groups. However, ASPH expression was robust and equal levels were found in tumors derived from all groups (Fig. 1G). More important, infiltration of $CD3^+$ T lymphocytes into HCC tumors was gradually increased in mice with PD1 blockade, to vaccine, to combination therapy, as compared to control (Fig. 1H). Thus, the combined therapy demonstrated anti-tumor effects that was higher than bearing animals given vaccine or PD-1 blockade alone (Fig. 1I). Importantly, anti-ASPH specific antibody (as an indicator of B cell response) could also be detected in vaccine and combination groups as expected, compared to control and PD-1 treated animals (Fig. 1J).

ASPH-MYC signaling upregulates PD-L1 expression on 4T1 breast cancer cells.

Consistent with previous studies(35, 36) in mice harboring TNBC generated by 4T1 cells, PD-L1 was upregulated in association with ASPH-MYC(14) expression as demonstrated by IHC (**Additional File 2: Fig. S2A**). In this context, there was also extensive metastatic spread to the lymph nodes, liver, spleen pancreas, diaphragm, adrenal glands and kidney as shown in **Additional File 2: Figure S2B**.

Phage vaccination targeting ASPH followed by PD-1 blockade significantly reduces TNBC tumor metastasis.

The TNBC breast cancer model demonstrates widespread metastasis as shown in **Additional File 2: Figure S2B-D**. Combination therapy significantly reduced total metastatic tumor burden produced by TNBC cells compared to control (**Additional File 2: Fig. S2E-F**). Primary tumor growth was also inhibited to a marked extent by treatment in the combination group (Fig. 2A). This anti-tumor effect was dose dependent on the concentration of anti-PD-1 administered (Fig. 2D). It was of interest that combination therapy blunted the development and growth of pulmonary metastasis (Fig. 2B-C). Compared to control, combination therapy also effected multiple-organ metastases of breast cancer. Metastatic lesions were also identified at different and distant sites such as liver, lymph nodes, spleen, adrenal gland, and kidney compared to control (**Additional File 2: Fig.S2C-G**). The high dose (200 μg) anti-PD-1 mAb demonstrates the most pronounced inhibitory effects on both size of primary tumor growth and number of pulmonary metastasis (Fig. 2A and 2E), compared to a low dose (12.5 μg).

Antigen specific activation of $CD8^+$ CTL and $CD4^+$ Th following l phage immunization in combination with PD-1 blockade.

There was an increase in ASPH CTL activity of splenocytes when compared to unvaccinated control. Administration of either anti-PD-1 mAb or vaccine alone generated intermediate responses. It was of

interest that ASPH-based λ phage vaccination was as effective as PD-1 blockade with respect to CTL activity against 4T1 cells (Fig. 3A).

The percentage of antigen (ASPH) specific $CD4^+$ and $CD8^+$ T cells that were activated in a splenocyte population was analyzed by flow cytometry (Fig. 3B). Both vaccine alone and combination therapy led to a substantial increase in ASPH specific $CD4^+$ and $CD8^+$ activity as measured by the secretion of IFN-γ after prior restimulation of splenocytes with phage vaccine and rASPH protein. The highest level of activity occurred in the combination group compared to either vaccine or PD-1 blockade alone.

Combination therapy induced a substantial increase in infiltration of $CD3^+$ T cells into the primary breast tumors that was produced by either PD-1 blockade or vaccine alone as compared to control (Fig. 3C-D). Likewise, combination therapy synergistically reduced pulmonary metastasis, compared to either vaccine or PD-1 blockade alone (Fig. 3E-F). Importantly, anti-ASPH specific antibody titers, as an index of B cell response, was detected in mice derived from vaccine and combination groups (Fig. 3G). Combination therapy contributed to enhanced infiltration of $CD8^+$ effector CTLs (Fig. 3H-J) and $CD45RO^+$ memory CTLs (Fig. 3K-M) among the $CD3^+$ TILs into both primary tumors and pulmonary metastases.

Characterization of the local microenvironment.

In response to combination therapy, $CD3^+$ TILs including $CD62L^+$ or $CD8^+$ effector CTLs and $CD45RO^+$ memory CTLs, were predominantly localized in the intra- and peritumoral tertiary lymphoid structures (TLSs) in close proximity to $CD4^+BCL\text{-}6^+$ T follicular helper cells (TFH) (Fig. 4A-C), $CD19^+$ B cell infiltrates (germinal center) (Fig. 4D-F), $CD21^+$ follicular dendritic cell (FDC)(37) (Fig. 4G-J). This TLS also facilitates activation and maturation of DCs highly expressing $LRP1^+$, $TLR4^+$ or LMP3 (Fig. 5A-J) in response to combination therapy. In most tumors treated with combination therapy, TILs surrounded the central B cell area and also at the tumor normal tissue interface, to suggest that TLSs are actively recruiting immune subsets to the tumor microenvironment (TME).

CXCL13-CXCR5 interactions with PD1-PDL1 inhibitory signal in HCC and TNBC.

In both HCC (**Additional File 3: Fig.S3;** Fig. 6A) and TNBC (**Additional File 4: Fig.S4;** Fig. 6B) animal models, PD-L1 was significantly upregulated on cancer cells whereas PD-1 was upregulated on TILs(38). In the control group, ASPH induced MYC activation mediated PD-L1 upregulation. It is hypothesized that $PD\text{-}L1^+$ cancer cells interacted with $PD\text{-}1^+$ TILs, leading to exhaustion and apoptosis of TILs in the TME; simultaneously, cancer cells will exhibit a more aggressive phenotype possibly attributed to autocrine, paracrine or endocrine CXCL13-CXCR5 interactions. The CXCL13 secreting $PD\text{-}1^+$ TILs were predominantly found in controls, which interacted with $CXCR5^+PD\text{-}L1^+$ cancer cells. However, $PD\text{-}1^+$ TILs may be impaired in classical effector function as shown in **Additional File 5: Figure S5A** and quantified in Figure 6. Upon combination treatment, PD-L1/PD-1 inhibitory signal and exhaustion of CTLs were substantially attenuated. In response to combination therapy, CXCL13 produced by $ASPH^+$ expressing cancer cells may be capable of recruiting immune cells, especially $CXCR5^+/CD8^+$ TILs (including CTLs),

to participate in forming TLSs and to execute cytotoxicity. Furthermore, CXCL13 produced by $CXCR5^+/CD8^+$ TILs (through autocrine, paracrine or endocrine) could directly bind and lyse $CXCR5^+$ tumor cells to induce cytotoxicity; simultaneously, as well as mediate recruitment of $CXCR5^+$ B and T_{FH} cells to help form the TLSs. The sspecific immune contexture characterized by TLSs confers sensitivity to combination therapy. Notably, in response to combination therapy, when ASPH-MYC as well as downstream PD-L1/PD-1 signals were blocked, CTLs secreted CXCL13 to bind CXCR5 on cancer cells so that CTLs could produce cytotoxicity against cancer cells efficiently (**Additional File 5: Fig.S5B;** quantified in Fig. 6).

Discussion

We have demonstrated that a λ phage vaccine construct expressing a N-terminal peptide of ASPH when combined with a checkpoint inhibitor substantially reduces both primary tumor growth and multi-organ metastasis in murine models of TNBC and HCC. The gpD fusion proteins of the l phage head are connected by linker peptide to N-terminal region of ASPH which allows the λ phage to display the specific protein that can be presented or cross-presented to the host immune cells(39). This system enables multiple copies of antigenic epitopes to be stably and efficiently displayed on the λ phage head even taken into account with low-affinity protein-protein interactions(39). We have recently identified anti-tumor effects of this λ phage vaccine that targets ASPH expressing HCC(33). In this setting, the recombinant l phage primes strong $CD8^+$ CTLs responses both *in vitro* and *in vivo* against ASPH epitopes. This vaccine also activates Th1 cells and elicits the production of antigen-specific antibodies without the addition of an adjuvant protein. Taken together, this ASPH-based λ phage vaccine now in combination with a PD-1 blockade produces a synergistic, potent anti-tumor immune response in two syngeneic murine models of TNBC and HCC.

The presence and composition of TLS in TNBC and HCC models have been explored and how TLS interacts with cellular immune components of the host to generate anti-tumor effect has been demonstrated. ASPH serves as a target for immunotherapy in HCC and TNBC and is partially dependent on the formation of TLS (**Additional File 6: Fig.S6**). Ectopic TLSs, similar in architecture to secondary lymphoid organs (SLOs), are classically defined as lymphoid aggregates forming in non-hematopoietic organs in response to chronic and non-resolving inflammatory processes, such as infection, graft rejection, autoimmune disease and more recently, cancer. Spontaneous TLSs have been documented in melanoma, lung, colorectal and breast cancer, and are generally indicative of a reduced risk of recurrence and they are associated with a favorable clinical outcome(23, 34, 40). It has been proposed that TLSs provide a local and essential microenvironment for generating anti-tumor cellular and humoral immune responses and are linked with a reduced risk of recurrence and improved clinical outcome(23, 34). The TLSs are principally involved in the antigen specific anti-tumor immune responses by allowing the generation of effector and central memory T cells and plasma cells. However, the role of TLSs in HCC pathogenesis is controversial as they have recently been shown to promote the growth of hepatocyte progenitor cells(41). It had been reported that intra-tumoral TLSs were associated with an increased risk

of late tumor relapse and portend a trend toward reduced survival after surgical resection(41). In a murine model of chronic NF-κB activation, TLSs was composed of a micro-niche to facilitate the growth of malignant hepatocyte progenitor cells through activation and secretion of pro-tumoral cytokines(41). Therefore, the pathological significance of TLSs in TNBC and HCC needs to be further explored.

In this study, intra-tumoral TLSs was associated with a better therapeutic response to vaccine immunization in combination with PD-1 blockade. Thus, TLSs could represent the existence of an *in situ*, active and effective anti-tumor immune response(42). It has been suggested that high levels of endothelial venules (HEVs) in malignant tissue promotes anti-tumor immunity by recruiting naive lymphocytes into TLS^+ TME, followed by extranodal priming of effector cells. The TLSs and chronic intratumoral inflammation have been reported to correlate with a tolerogenic TME, and promotes tumor aggressiveness(43, 44).

An anti-PD-1 antibody, nivolumab, has been approved for the treatment of HCC in patients that have been previously treated with the kinase inhibitor sorafenib. Intra-tumoral infiltration by immune cells is a predictor of sensitivity to PDL-L1/PD-1 checkpoint inhibitors, as these drugs may enhance the *in situ* anti-tumor responses and overcome immune evasion. We have observed that intra-tumoral TLSs are sensitive to immunomodulating therapeutic strategies(42). Importantly, ASPH activates Notch signaling, to upregulate MYC expression, which in turn upregulates PD-L1(35, 45). The MYC-mediated activation of the PD-L1 gene has been shown to promote the liver cancer cell escape from the immune response(45). In addition, we suggest that PD-L1 expression on tumor cells has been upregulated by signaling through ASPH-Notch-MYC in both murine TNBC and HCC animal models. We found that PD-1 blockade was effective when administered in combination with a λ phage vaccine that targeted epitopes residing in the N-terminal peptide of ASPH. This finding suggests that the TME may be improved for T cell penetration and function(46–48).

In our study, CXCL13/CXCR5 axis interacts with the PD1-PDL1 inhibitory signal and playing a critical role in tumor progression and response to immunotherapy. In the absence of PD-1 inhibitor, CXCL13 ligand secreted by cancer cells binds to CXCR5 receptors and promotes an aggressive tumor phenotype. Simultaneously, CXCL13 derived from cancer cells binding CXCR5 on T cells may enhance PD1/PDL1 mediated exhaustion resulting in apoptosis of effector lymphocytes as shown by the diagram in Additional File 5: **Additional File 5: Figure S5**. In the presence of PD1 inhibitor, PD-L1 (on cancer cells)/PD-1 (on T cells) generated inhibitory signal is blocked. Effector T cells are activated and survive dependent on autocrine CXCL13/CXCR5 binding. T cells secrete CXCL13 to recruit $CXCR5^+$ immune cells, thus initiating an anti-tumor immune response. Cancer cells are subject to apoptosis when exposed to $CXCL13^+$ T cells(49, 50).

This λ phage vaccine could be employed for both cancer prevention and treatment. It is designed to specifically target ASPH using bacteriophage surface-expressed ASPH N-terminal peptides bound by a linker protein. This formulation is highly immunogenic and appears to overcome self-antigen tolerance by

providing a novel antigen presentation mode with inherent adjuvant properties; further studies will be required.

Vaccination with a λ phage-displaying ASPH peptides has various advantages. First, multiple copies of peptides are displayed on the same λ phage head particle. Once the initial phage display has been made and stocks have been stored, subsequent production is straight forward and less complicated than having to produce coupling peptides to carriers. Phage-displayed peptides can access both MHC class I and II pathways. Thus, λ phage display vaccines can stimulate both cellular and humoral immune responses, although as extracellular antigens, it would be expected that the majority of immune responses generated will be antibody biased. Particulate antigens, including phage, can access the MHC class I pathway through cross presentation and priming, suggesting that this process is likely to be involved for stimulating an adaptive cellular immune response by $CD8^+$ T cells to eliminate tumor cells. This λ phage can also act as a nonspecific immune stimulator attributed to a combination of foreign DNA (possibly due to CpG motifs) and repeating peptide motif coating the phage head.

The murine expressing BNL cell line produces robust growth when implanted subcutaneously into syngeneic BALB/c mice. Inoculated animals rapidly develop HCC and have to be euthanized as early as 5–6 weeks after implantation due to a large tumor burden with a poorly differentiated phenotype(8). The level of ASPH expression in BNL cell induced tumors is robust and in the same range observed in naturally occurring human HCC(8). Using this HCC murine model, a λ phage vaccine construct which displays the N-terminal protein of ASPH modestly inhibits subcutaneous tumor growth and progression. However, antitumor effects are substantially amplified by a simultaneous administered of a checkpoint PD-1 inhibitor. A prophylactic immunization schedule could be envisioned prior to surgical resection of the HCC tumor mass to prevent early disease reoccurrence and to inhibit the development and progression of established micro-metastatic disease. We hypothesize that residual tumor cells that may exist following surgery could be abolished or reduced by the host immune responses generated from this λ phage vaccine and checkpoint inhibitor given in combination.

Conclusions

Taken together, this combination immunotherapy stimulates an adaptive immune response to a single chemically defined protein that is highly expressed on the cellular surface of a wide majority of malignancies. This combination strikingly reduces the number and size of metastasis to various regions and particularly the lung, which was unanticipated. A possible mechanism for the observed anti-tumor effects is the known inhibition of tumor cell migration, invasion and now metastasis when the function of ASPH is altered by inhibition of enzymatic activity or is reduced in amount on the cell surface. Such a combination may have widespread application to solid tumors, such as liver, pancreas, gastric, esophageal, breast, cholangiocarcinoma and sarcomas since these tumors also highly overexpress ASPH as well.

Collectively, a λ phage vaccine targeting ASPH combined with a checkpoint inhibitor successfully initiates antigen specific $CD8^+$T and B cell-mediated cellular and humoral immunity in HCC and TNBC. This approach overcomes immunologic tolerance since ASPH is an oncofetal protein and thus an ideal TAA. We are led to believe that combined therapy allows ASPH peptides to be recognized, taken up, processed and presented as well as cross-presented by DCs since the l phage acts as an adjuvant to display tumor restricted molecules such as ASPH. These findings have potential for a potent and broad-spectrum therapy of a wide variety of aggressive solid human tumors.

Abbreviations

ASPH: aspartate β-hydroxylase

CTL: cytotoxic T lymphocyte

CXCL13: Chemokine ligand 13

CXCR5: C-X-C chemokine receptor type 5

DC: dendritic cell

FDC: follicular dendritic cell

GC: germinal center

HEV: high endothelial venules

HCC: hepatocellular carcinoma

IHC: immunohistochemistry

IPF: intermediate-power field

PD1: programmed cell death protein 1

PD-L1: programmed death-ligand 1

TAA: tumor associated antigen

TFH: follicular B helper T cell

TIL: tumor infiltrating lymphocyte

TLS: tertiary lymphoid structures

TME: tumor-microenvironment

TNBC: triple-negative breast cancer

Declarations

Ethics approval and consent to participate

For orthotopic TNBC and subcutaneous HCC models, all of the animal experiments were approved by the Institutional Animal Care and Use Committee of Rhode Island Hospital, CMTT# 0240-16.

Consent for publication

Not applicable.

Availability of data and materials

The datasets used and/or analyzed during the current study are available from the corresponding author on reasonable request.

Competing Interests

The authors have no conflicts of interest to declare.

Funding

This work was supported in part by National Institutes of Health (NIH) (Grant numbers CA123544, P30GM110759) and Institutional Funds.

Author's contributions

Conceptualization: X.Q.D., J.R.W.

Methodology: X.W.B., Y.M.Z, Y.Y., Y.M., H.G.

Statistical analysis: X.W.B., Y.M.Z, Y.Y., Y.M., N.M., H.H.

Investigation: X.W.B., Y.M.Z, Y.Y., Y.M., B.Z., N.M., H.H., R.C., S.Z., B.S.

Writing –Original Draft: X.W.B., X.Q.D

Writing –Review & Editing: Y.M.Z, Y.Y., Y.M., B.Z., N.M., H.H., R.C., S.Z., B.S., H.G., J.R.W.

Funding Acquisition: X.Q.D, J.R.W.

Resources: X.Q.D, J.R.W., H.G.

Supervision: X.Q.D, J.R.W.

Acknowledgements

We highly appreciate Flow Cytometry and Sorting Facility at Brown University for providing technical assistance.

References

1. Siegel RL, Miller KD, Jemal A. Cancer statistics, 2018. CA: a cancer journal for clinicians. 2018;68(1):7-30.
2. Alsaab HO, Sau S, Alzhrani R, Tatiparti K, Bhise K, Kashaw SK, et al. PD-1 and PD-L1 Checkpoint Signaling Inhibition for Cancer Immunotherapy: Mechanism, Combinations, and Clinical Outcome. Front Pharmacol. 2017;8:561.
3. Postow MA, Sidlow R, Hellmann MD. Immune-Related Adverse Events Associated with Immune Checkpoint Blockade. The New England journal of medicine. 2018;378(2):158-68.
4. Lavaissiere L, Jia S, Nishiyama M, de la Monte S, Stern AM, Wands JR, et al. Overexpression of human aspartyl(asparaginyl)beta-hydroxylase in hepatocellular carcinoma and cholangiocarcinoma. The Journal of clinical investigation. 1996;98(6):1313-23.
5. Aihara A, Huang CK, Olsen MJ, Lin Q, Chung W, Tang Q, et al. A cell-surface beta-hydroxylase is a biomarker and therapeutic target for hepatocellular carcinoma. Hepatology. 2014;60(4):1302-13.
6. Tomimaru Y, Mishra S, Safran H, Charpentier KP, Martin W, De Groot AS, et al. Aspartate-beta-hydroxylase induces epitope-specific T cell responses in hepatocellular carcinoma. Vaccine. 2015;33(10):1256-66.
7. Noda T, Shimoda M, Ortiz V, Sirica AE, Wands JR. Immunization with aspartate-beta-hydroxylase-loaded dendritic cells produces antitumor effects in a rat model of intrahepatic cholangiocarcinoma. Hepatology. 2012;55(1):86-97.
8. Shimoda M, Tomimaru Y, Charpentier KP, Safran H, Carlson RI, Wands J. Tumor progression-related transmembrane protein aspartate-beta-hydroxylase is a target for immunotherapy of hepatocellular carcinoma. Journal of hepatology. 2012;56(5):1129-35.
9. Ince N, de la Monte SM, Wands JR. Overexpression of human aspartyl (asparaginyl) beta-hydroxylase is associated with malignant transformation. Cancer research. 2000;60(5):1261-6.
10. de la Monte SM, Tamaki S, Cantarini MC, Ince N, Wiedmann M, Carter JJ, et al. Aspartyl-(asparaginyl)-beta-hydroxylase regulates hepatocellular carcinoma invasiveness. Journal of hepatology. 2006;44(5):971-83.
11. Cantarini MC, de la Monte SM, Pang M, Tong M, D'Errico A, Trevisani F, et al. Aspartyl-asparagyl beta hydroxylase over-expression in human hepatoma is linked to activation of insulin-like growth factor and notch signaling mechanisms. Hepatology. 2006;44(2):446-57.
12. Ogawa K, Lin Q, Li L, Bai X, Chen X, Chen H, et al. Aspartate beta-hydroxylase promotes pancreatic ductal adenocarcinoma metastasis through activation of SRC signaling pathway. J Hematol Oncol. 2019;12(1):144.

13. Iwagami Y, Huang CK, Olsen MJ, Thomas JM, Jang G, Kim M, et al. Aspartate beta-hydroxylase modulates cellular senescence through glycogen synthase kinase 3beta in hepatocellular carcinoma. Hepatology. 2016;63(4):1213-26.
14. Dong X, Lin Q, Aihara A, Li Y, Huang CK, Chung W, et al. Aspartate beta-Hydroxylase expression promotes a malignant pancreatic cellular phenotype. Oncotarget. 2015;6(2):1231-48.
15. Lin Q, Chen X, Meng F, Ogawa K, Li M, Song R, et al. Multi-organ metastasis as destination for breast cancer cells guided by biomechanical architecture. Am J Cancer Res. 2021;11(6):2537-67.
16. Lin Q, Chen X, Meng F, Ogawa K, Li M, Song R, et al. ASPH-notch Axis guided Exosomal delivery of Prometastatic Secretome renders breast Cancer multi-organ metastasis. Molecular cancer. 2019;18(1):156.
17. Ogawa K, Lin Q, Li L, Bai X, Chen X, Chen H, et al. Prometastatic Secretome Trafficking via Exosomes Initiates Pancreatic Cancer Pulmonary Metastasis. Cancer letters. 2020.
18. Chung W, Kim M, de la Monte S, Longato L, Carlson R, Slagle BL, et al. Activation of signal transduction pathways during hepatic oncogenesis. Cancer letters. 2016;370(1):1-9.
19. Nagaoka K, Bai X, Ogawa K, Dong X, Zhang S, Zhou Y, et al. Anti-tumor activity of antibody drug conjugate targeting aspartate-beta-hydroxylase in pancreatic ductal adenocarcinoma. Cancer letters. 2019;449:87-98.
20. Wang K, Liu J, Yan ZL, Li J, Shi LH, Cong WM, et al. Overexpression of aspartyl-(asparaginyl)-beta-hydroxylase in hepatocellular carcinoma is associated with worse surgical outcome. Hepatology. 2010;52(1):164-73.
21. Maeda T, Taguchi K, Aishima S, Shimada M, Hintz D, Larusso N, et al. Clinicopathological correlates of aspartyl (asparaginyl) beta-hydroxylase over-expression in cholangiocarcinoma. Cancer detection and prevention. 2004;28(5):313-8.
22. Fridman WH, Pages F, Sautes-Fridman C, Galon J. The immune contexture in human tumours: impact on clinical outcome. Nature reviews Cancer. 2012;12(4):298-306.
23. Fridman WH, Zitvogel L, Sautes-Fridman C, Kroemer G. The immune contexture in cancer prognosis and treatment. Nature reviews Clinical oncology. 2017;14(12):717-34.
24. Sanmamed MF, Chen L. A Paradigm Shift in Cancer Immunotherapy: From Enhancement to Normalization. Cell. 2018;175(2):313-26.
25. Bruni D, Angell HK, Galon J. The immune contexture and Immunoscore in cancer prognosis and therapeutic efficacy. Nature reviews Cancer. 2020;20(11):662-80.
26. Sautes-Fridman C, Petitprez F, Calderaro J, Fridman WH. Tertiary lymphoid structures in the era of cancer immunotherapy. Nature reviews Cancer. 2019;19(6):307-25.
27. Munoz-Erazo L, Rhodes JL, Marion VC, Kemp RA. Tertiary lymphoid structures in cancer - considerations for patient prognosis. Cell Mol Immunol. 2020;17(6):570-5.
28. Galon J, Bruni D. Approaches to treat immune hot, altered and cold tumours with combination immunotherapies. Nature reviews Drug discovery. 2019;18(3):197-218.

29. Aghebati-Maleki L, Bakhshinejad B, Baradaran B, Motallebnezhad M, Aghebati-Maleki A, Nickho H, et al. Phage display as a promising approach for vaccine development. J Biomed Sci. 2016;23(1):66.
30. Adhya S, Merril CR, Biswas B. Therapeutic and prophylactic applications of bacteriophage components in modern medicine. Cold Spring Harb Perspect Med. 2014;4(1):a012518.
31. Smith GP. Filamentous fusion phage: novel expression vectors that display cloned antigens on the virion surface. Science. 1985;228(4705):1315-7.
32. Yang F, Forrer P, Dauter Z, Conway JF, Cheng N, Cerritelli ME, et al. Novel fold and capsid-binding properties of the lambda-phage display platform protein gpD. Nat Struct Biol. 2000;7(3):230-7.
33. Iwagami Y, Casulli S, Nagaoka K, Kim M, Carlson RI, Ogawa K, et al. Lambda phage-based vaccine induces antitumor immunity in hepatocellular carcinoma. Heliyon. 2017;3(9):e00407.
34. Calderaro J, Petitprez F, Becht E, Laurent A, Hirsch TZ, Rousseau B, et al. Intra-tumoral tertiary lymphoid structures are associated with a low risk of early recurrence of hepatocellular carcinoma. Journal of hepatology. 2019;70(1):58-65.
35. Casey SC, Tong L, Li Y, Do R, Walz S, Fitzgerald KN, et al. MYC regulates the antitumor immune response through CD47 and PD-L1. Science. 2016;352(6282):227-31.
36. Lin CY, Loven J, Rahl PB, Paranal RM, Burge CB, Bradner JE, et al. Transcriptional amplification in tumor cells with elevated c-Myc. Cell. 2012;151(1):56-67.
37. Thommen DS, Koelzer VH, Herzig P, Roller A, Trefny M, Dimeloe S, et al. A transcriptionally and functionally distinct PD-1(+) CD8(+) T cell pool with predictive potential in non-small-cell lung cancer treated with PD-1 blockade. Nature medicine. 2018;24(7):994-1004.
38. Zheng C, Zheng L, Yoo JK, Guo H, Zhang Y, Guo X, et al. Landscape of Infiltrating T Cells in Liver Cancer Revealed by Single-Cell Sequencing. Cell. 2017;169(7):1342-56 e16.
39. Gupta A, Onda M, Pastan I, Adhya S, Chaudhary VK. High-density functional display of proteins on bacteriophage lambda. J Mol Biol. 2003;334(2):241-54.
40. Dieu-Nosjean MC, Giraldo NA, Kaplon H, Germain C, Fridman WH, Sautes-Fridman C. Tertiary lymphoid structures, drivers of the anti-tumor responses in human cancers. Immunol Rev. 2016;271(1):260-75.
41. Finkin S, Yuan D, Stein I, Taniguchi K, Weber A, Unger K, et al. Ectopic lymphoid structures function as microniches for tumor progenitor cells in hepatocellular carcinoma. Nat Immunol. 2015;16(12):1235-44.
42. Johansson-Percival A, He B, Li ZJ, Kjellen A, Russell K, Li J, et al. De novo induction of intratumoral lymphoid structures and vessel normalization enhances immunotherapy in resistant tumors. Nat Immunol. 2017;18(11):1207-17.
43. Joshi NS, Akama-Garren EH, Lu Y, Lee DY, Chang GP, Li A, et al. Regulatory T Cells in Tumor-Associated Tertiary Lymphoid Structures Suppress Anti-tumor T Cell Responses. Immunity. 2015;43(3):579-90.

44. Shields JD, Kourtis IC, Tomei AA, Roberts JM, Swartz MA. Induction of lymphoidlike stroma and immune escape by tumors that express the chemokine CCL21. Science. 2010;328(5979):749-52.
45. MYC-Mediated Translation of PD-L1 Promotes Liver Cancer Immune Escape. Cancer discovery. 2019;9(3):317.
46. Schmittnaegel M, Rigamonti N, Kadioglu E, Cassara A, Wyser Rmili C, Kiialainen A, et al. Dual angiopoietin-2 and VEGFA inhibition elicits antitumor immunity that is enhanced by PD-1 checkpoint blockade. Science translational medicine. 2017;9(385).
47. Allen E, Jabouille A, Rivera LB, Lodewijckx I, Missiaen R, Steri V, et al. Combined antiangiogenic and anti-PD-L1 therapy stimulates tumor immunity through HEV formation. Science translational medicine. 2017;9(385).
48. Tang H, Wang Y, Chlewicki LK, Zhang Y, Guo J, Liang W, et al. Facilitating T Cell Infiltration in Tumor Microenvironment Overcomes Resistance to PD-L1 Blockade. Cancer cell. 2016;29(3):285-96.
49. Kazanietz MG, Durando M, Cooke M. CXCL13 and Its Receptor CXCR5 in Cancer: Inflammation, Immune Response, and Beyond. Front Endocrinol (Lausanne). 2019;10:471.
50. Nagarsheth N, Wicha MS, Zou W. Chemokines in the cancer microenvironment and their relevance in cancer immunotherapy. Nat Rev Immunol. 2017;17(9):559-72.

Figures

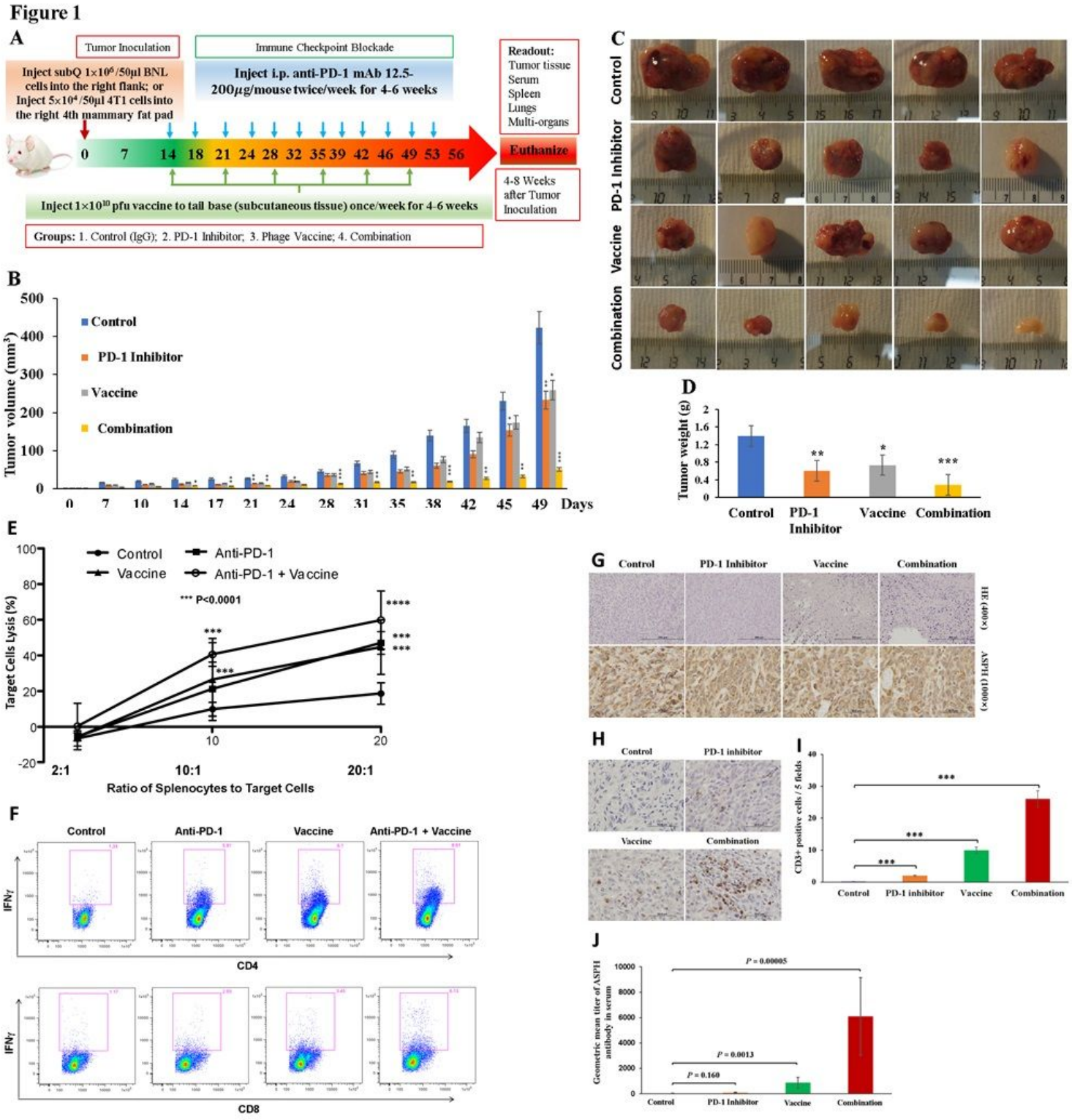

Figure 1

Therapeutic effects of different treatments on tumor development and progression in a murine subcutaneous model of HCC. (A) Example of an experimental protocol for a murine subcutaneous model of liver (HCC) and breast cancer (TNBC) generated by injecting ASPH-expressing BNL cells subcutaneously and 4T1 cells orthotopically (mammary fat pad), respectively. For each model, Balb/C mice were randomly divided to 4 groups (n=6/group): control, PD1 blockade (anti-PD-1 mAb), ASPH-

based λ phage vaccine, and combination (PD-1 blockade + vaccine). (B) Growth curves of HCC tumors generated by subcutaneous injection of BNL cells into Balb/c mice. Note the substantial anti-tumor effect of combination therapy (also see Figure S1B). (C) Macroscopic appearance of resected HCC tumors. (D) Tumor weights of HCC after 49 days in the 4 treatment groups. (E) Demonstration of in vitro cytotoxicity of splenocytes derived from mice against target BNL cells. (F) Antigen (ASPH) specific CD4+ and CD8+ T cell activation as demonstrated by upregulation of IFN-γ. (G) Histological features of ASPH expression in HCC tumors. (H-I) Number of CD3+ tumor infiltrating lymphocytes (TILs) in HCC tumors. (J) Anti-ASPH antibody titers in serum derived from different groups. *, p<0.05; **, p<0.01; ***, p<0.005; ****, p<0.001.

Figure 2

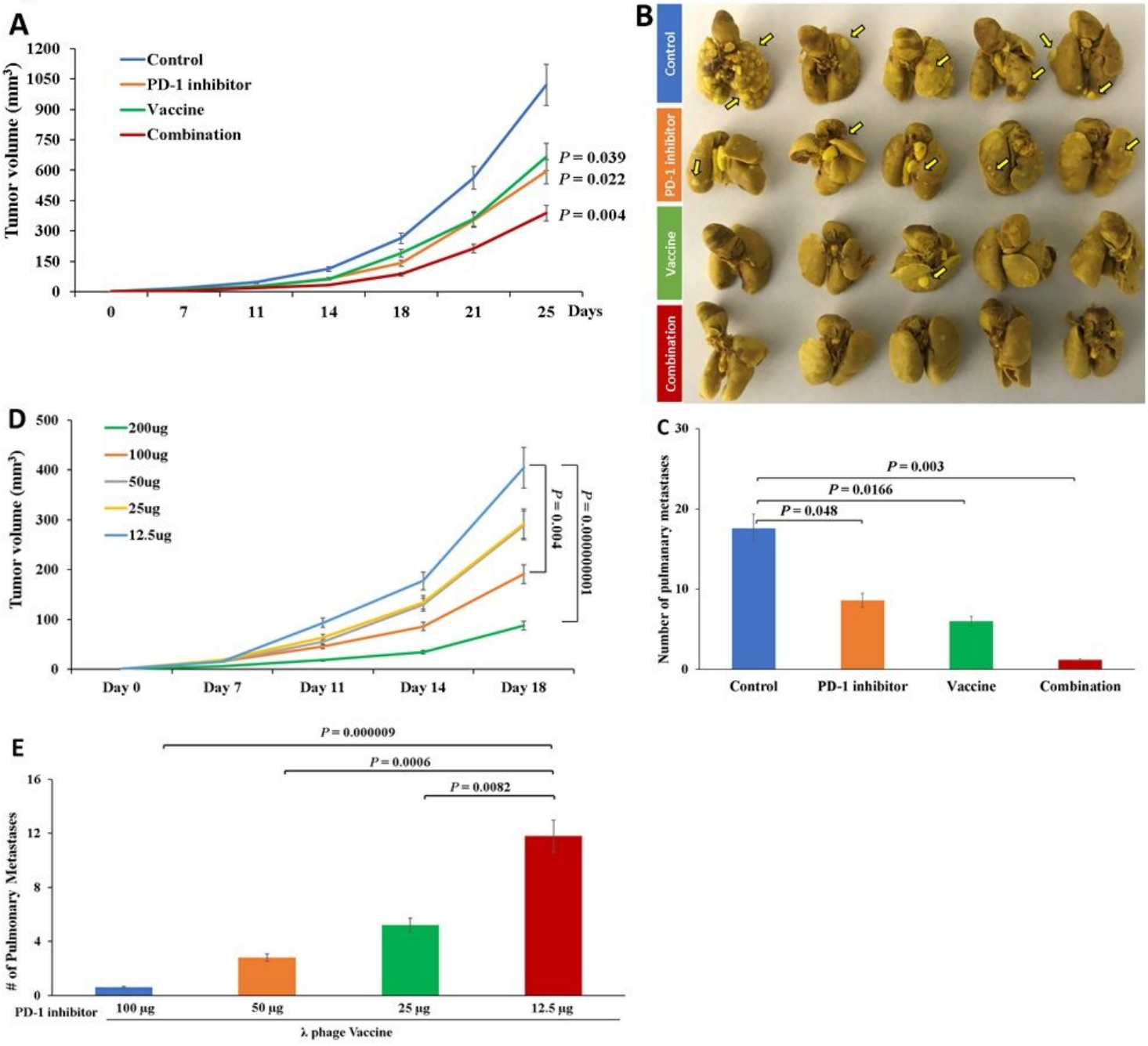

Figure 2

Anti-tumor effects of different reagents on tumor development and metastasis in an orthotopic model generated by 4T1 cells in Balb/C mice. (A) Growth curves of primary TNBC tumors. (B) Gross appearance of lungs harboring metastatic TNBC tumors. (C) Number of pulmonary metastatic tumors in mice derived from the different groups. (D) Dose-dependent inhibitory effects of anti-PD-1 mAb on TNBC tumor growth in λ phage vaccinated mice as compared to the low dose group (12.5μg), *** $p<0.001$; ****$p<0.000000001$. (E) Dose-dependent inhibitory effects of anti-PD-1 mAb on pulmonary metastases in λ phage vaccinated mice. Comparisons were made to 4 different concentrations of anit-PD-1 mAb. *, $p<0.05$; **, $p<0.01$; ***, $p<0.005$; ****, $p<0.001$.

Figure 3

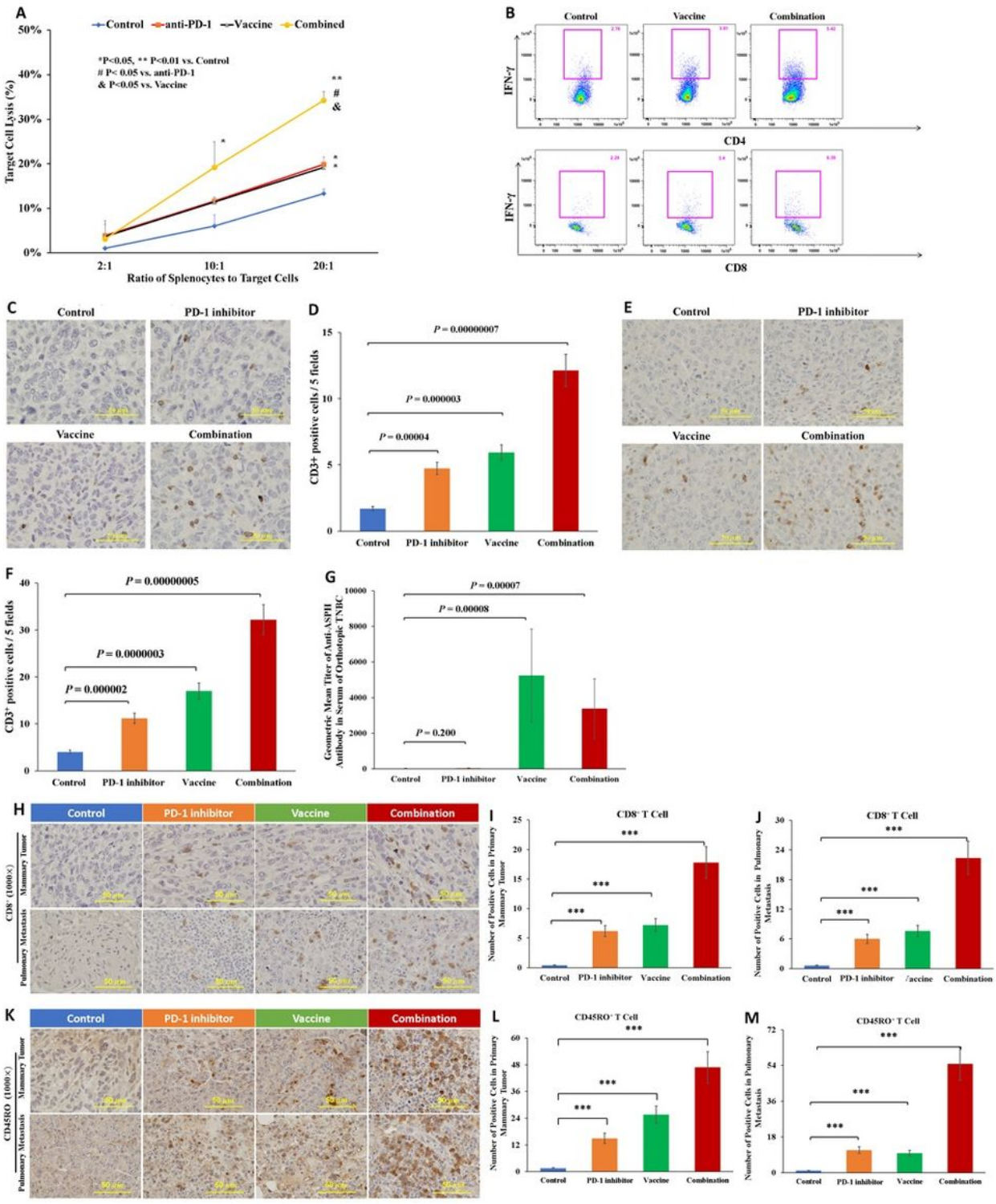

Figure 3

Activation of antigen specific TILs and B cells in the TNBC metastatic model of breast cancer. (A) In vitro cytotoxicity of splenocytes towards 4T1 cells. (B) Generation of antigen (ASPH) specific CD4+ and CD8+ T cells as demonstrated by upregulation of IFNγ. (C-D) Number of CD3+ TILs in TNBC primary tumors and (E-F) pulmonary metastases. (G) ASPH specific antibody titers in serum derived from the 4 treatment groups. (H-J) Number of CD62L+/CD8+ effector CTLs in primary tumors and pulmonary metastases. (K-

M) Number of CD45RO+ memory CTLs in primary tumors and pulmonary metastases. *, p<0.05; **, p<0.01; ***, p<0.005; ****, p<0.001.

Figure 4

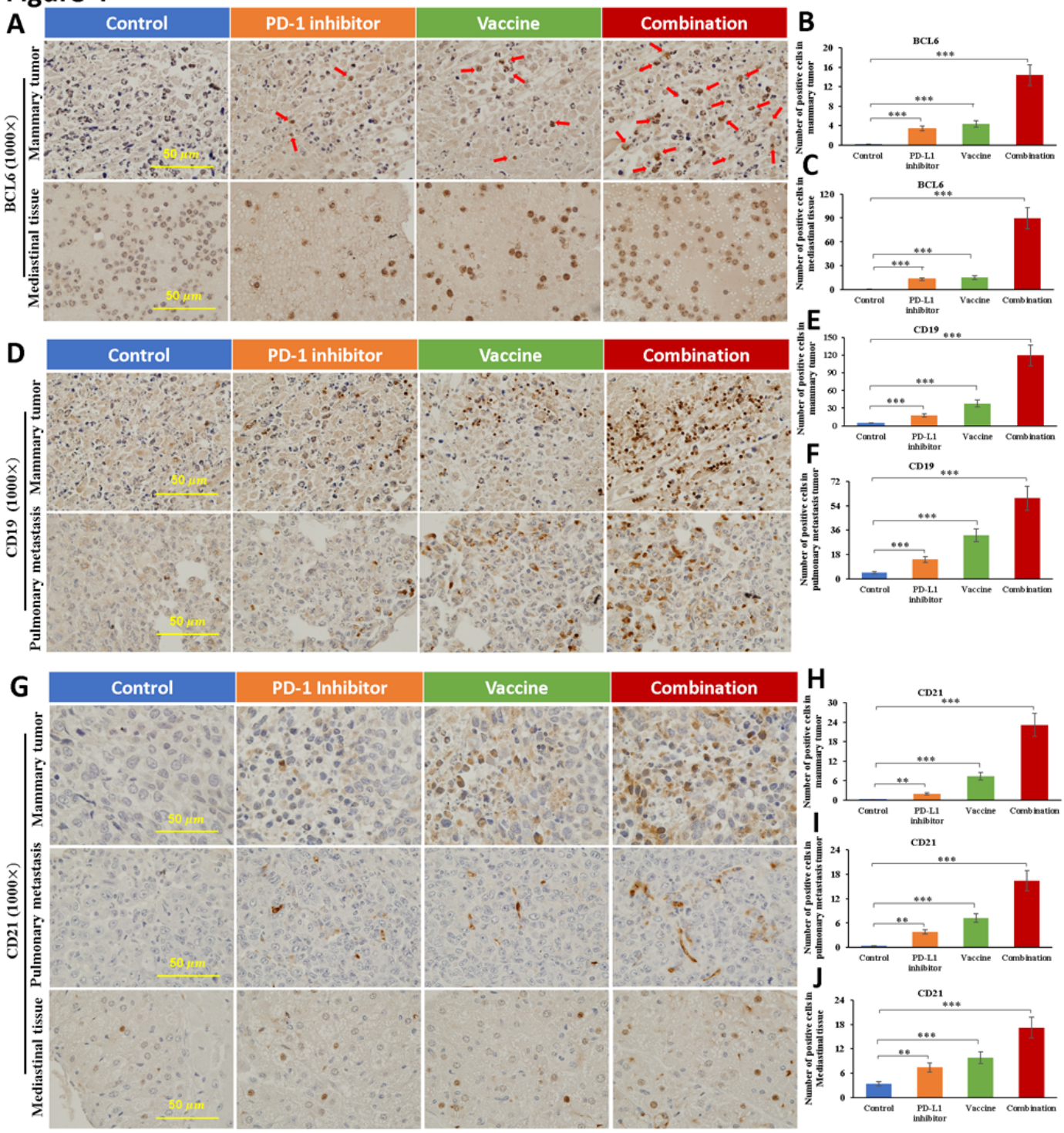

Figure 4

Intra-tumor TLS in 4T1 TNBC breast cancer tumors. (A-C) Number of CD4+/BCL6+ T follicular helper cell (TFH) population located in primary tumors and mediastinal metastases. (D-F) Number of CD19+ B population in primary tumors and pulmonary metastases. (G-J) Number of CD21+ follicular dendritic cell

(FDC) population in primary mammary tumors as well as mediastinal and pulmonary metastases. *, p<0.05; **, p<0.01; ***, p<0.005; ****, p<0.001.

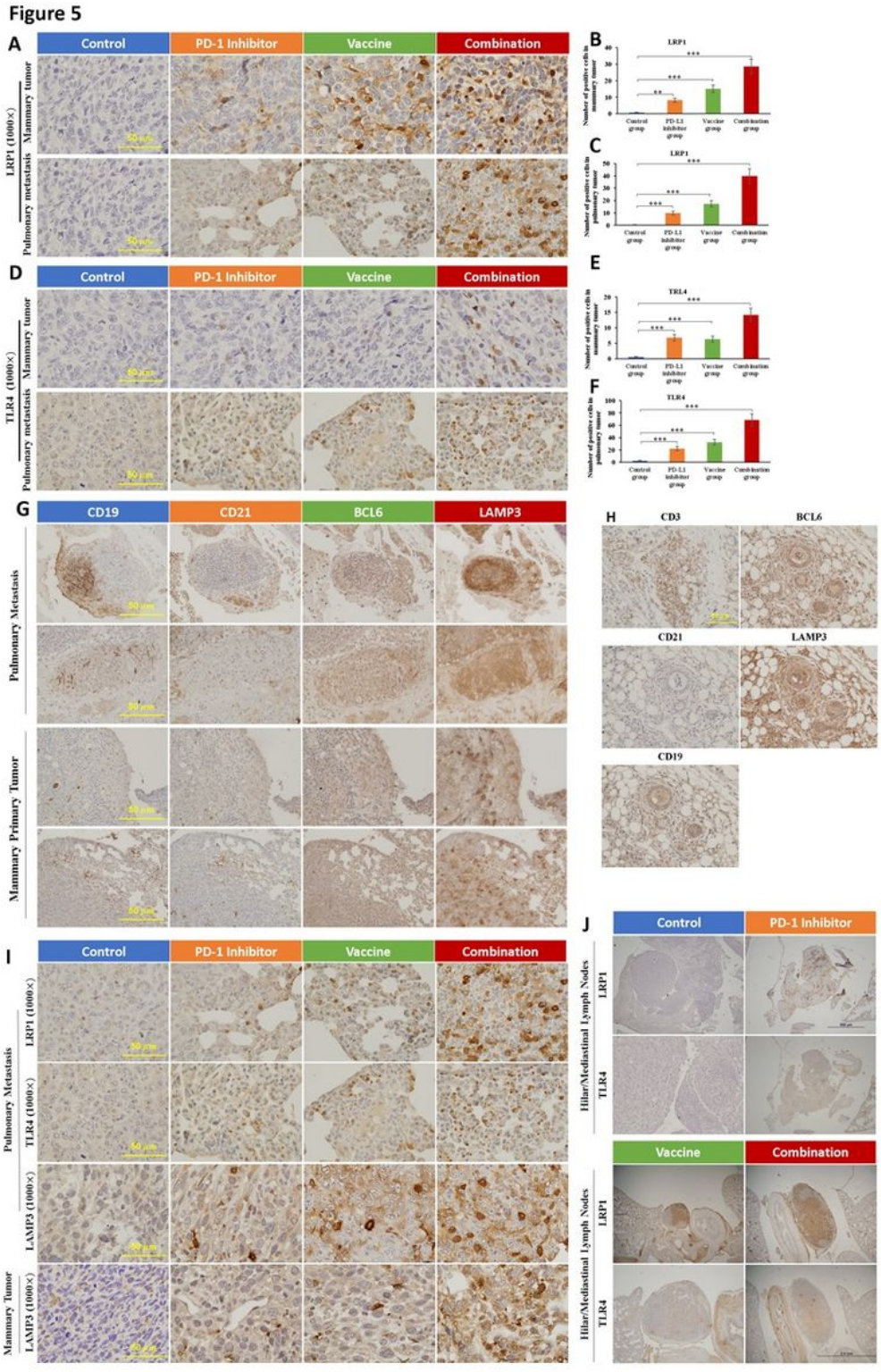

Figure 5

Activation and maturation of DCs are attributed to TLSs. (A-C) Number of LRP1+ DCs population in primary tumors and mediastinal metastases. (D-F) Number of TLR4+ DCs population in primary tumors and pulmonary metastases. (G) Intra-tumoral TLSs in primary mammary tumors and metastases induced

by combination therapy. (H) Peri-tumoral TLSs (colocalized with CD3+ TILs) induced by combinatory therapy. (I) LAMP3+ / LRP1+/ TLR4+ DCs population in primary tumors and pulmonary metastases. (J) LRP1+/ TLR4+ DCs population in hilar/mediastinal lymph nodes metastases. *, p<0.05; **, p<0.01; ***, p<0.005; ****, p<0.001.

Figure 6

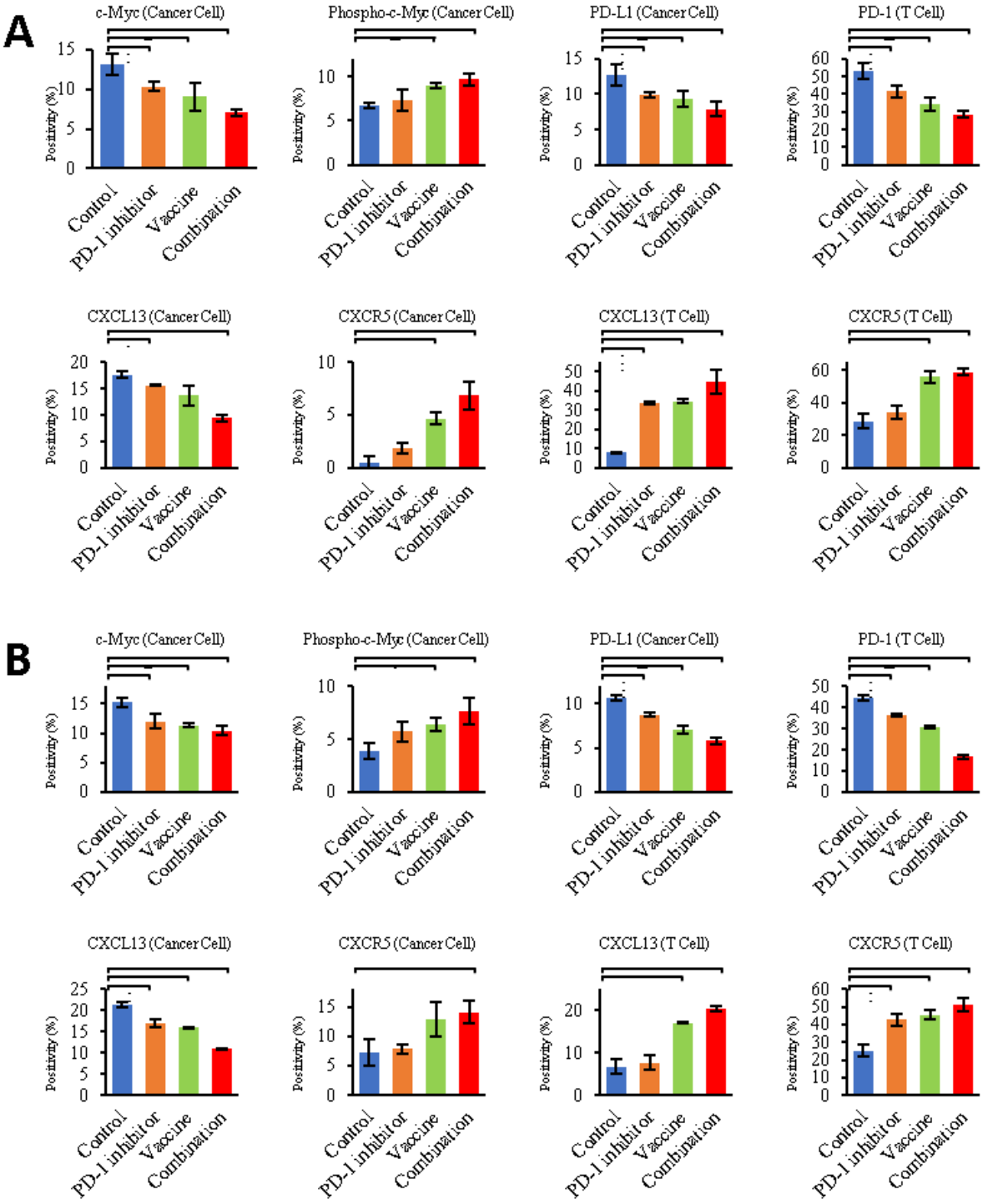

Figure 6

Expression profiling of major components involved in PD-1/PD-L1 inhibitory signal and CXCL13-CXCR5 axis in HCC and TNBC. As stratified by therapeutic strategies, differential expression levels of MYC, activated (phosphorylated) MYC, PD-1, PD-L1, CXCL13 and CXCR5 can be detected in (A) HCC and (B) TNBC tumor cells or stroma (TME). *, $p<0.05$; **, $p<0.01$; ***, $p<0.005$; ****, $p<0.001$.

Supplementary Files

This is a list of supplementary files associated with this preprint. Click to download.

- FigureS1.tif
- FigureS2.tif
- FigureS3.tif
- FigureS4.tif
- FigureS5.tif
- FigureS6.tif
- SupplementalInformation.docx